# Brain Resting-State Networks in Adolescents with High Functioning Autism: Analysis of Connectivity and Neurodynamics

Antoine Bernas[a,*], Evelien M. Barendse[b,d,e], Albert P. Aldenkamp[a,b,d], Jacob F.A. Jansen[b,c], Marc P.H. Hendriks[e], Roy P.C. Kessels[e,f], Frans M.J. Willems[a], Peter H.N. de With[a], Svitlana Zinger[a,d]

[a] *Department of Electrical Engineering, Signal Processing Systems, Eindhoven University of Technology, Eindhoven, the Netherlands;*
[b] *Department of Neurology, School for Mental Health and Neuroscience, Maastricht University Medical Center, the Netherlands;*
[c] *Department of Radiology, Cognitive Neuropsychiatry and Clinical Neuroscience, Maastricht University Medical Center, the Netherlands;*
[d] *Department of Behavioral Sciences, Epilepsy Center Kempenhaeghe, Heeze, the Netherlands;*
[e] *Donders Institute for Brain, Cognition and Behaviour, Radboud University Nijmegen, the Netherlands;*
[f] *Department of Medical Psychology, Radboud University Nijmegen Medical Centre, Nijmegen, The Netherlands.*

**Abstract**

Autism Spectrum Disorder (ASD) is characterized mainly by functional and communication impairments as well as restrictive and repetitive behavior. On one end of the spectrum, High Functioning Autism (HFA) is definied as ASD with intelligence scores within the normal or above it ($\geq$ 80). The leading hypothesis for the neural basis of autism postulates globally abnormal brain connectivity. Several functional Magnetic Resonance Imaging (fMRI) studies focused on connectivity in the context of psychological tasks. However, even in the absence of a task, the brain exhibits a high degree of functional connectivity, known as intrinsic, or resting-state, connectivity. Over the past decade, many resting-state investigations on different brain areas or regions of interest of people with autism showed conflicting results in connectivity. Thus, global default connectivity in individuals with autism and typically developing (TD) controls is not well characterized, which is especially valid for a high-functioning young population with ASD.
The aim of this study is to test whether HFA adolescents have an abnormal resting-state functional connectivity. We performed spatial and temporal analyses on Resting-State Networks (RSNs) for the groups of 13 ASD adolescents and 13 neurotypically IQ- and age-matched controls. For the spatial analysis, we used probabilistic Independent Component Analysis (ICA) and a permutation statistical method to discover the RSN differences between the groups. For the temporal analysis, we applied Granger causality in order to find differences in neurodynamics. Controls and high-functioning adolescents with autism display very similar patterns and strengths of resting-state connectivity. We do not find any significant differences between ASD and controls in the spatial resting state connectivity. However, in the temporal dynamics of this connectivity, we found interesting differences in the causal effect properties of RSNs made of temporal and prefontal cortices. This results lead us to the conclusion that this temporal dynamic difference of these RSNs between individuals with HFA and TD controls is subtle and seems to be triggered by a prescient cognitive task.

*Keywords:* `Autism Spectrum Disorder, High Functioning Austim, functional MRI, resting state brain connectivity, Independent Component Analysis Granger causality, neurodynamics`

## 1. Introduction

Autism Spectrum Disorder (ASD) is a range of complex neurodevelopmental syndromes defined by the presence of social impairments, communication abnormalities, and restricted, stereotyped and repetitive behavior. Autistic Disorder (also called classic ASD), Asperger syndrome and Pervasive Developmental Disorders – Not Otherwise Specified (PDD-NOS) are considered as subtypes of ASD (Barendse et al., 2013). On one end of the spectrum, the low-prevalence autistic syndrome defined as High-Functioning Autism is characterized by intelligence scores (IQ) of 80 or above, and often associate with Asperger's Syndrome which exhibit no severe global cognitive developmental impairment and no anomalies in spoken language (Soulière et al., 2011).

Recently, increasing interest is focused on abnormalities in (functional) brain organization in ASD. Especially, fMRI-based brain connectivity research was considered as a target. Most reports on underconnectivity in autism have focused on specific brain regions or networks related to cognitive functions such as working memory, executive function, visual attention and language processing (Anderson et al., 2011; Cherkassky et al., 2006). Many task-based functional fMRI studies report that ASD is associated with either weaker or stronger connectivity between various structures (Monk et al., 2009). However, focusing on the 'resting state' (i.e without task, brain at rest) in

*Corresponding author
*Email address:* `a.b.bernas@tue.nl` (Antoine Bernas )

fMRI provides a new domain to measure cortical synchronization. Indeed, in the past decade, functional connectivity of resting-state fMRI data is rapidly emerging as a highly efficient and powerful tool for in vivo mapping of neural circuitry in human brain (Zuo et al., 2011).
Recent resting-state functional connectivity MRI studies in autism provide inconsistent results (Möller et al., 2011). One of the reason for this is that these connectivity studies concentrate on a small number of brain regions or specific brain networks, instead of assessing the whole brain. (Tyszka et al., 2013).

Seed-based correlation represents the dominant approach for studying resting-state functional connectivity. Even though this approach has proven to be a powerful, efficient and reliable tool for neuroimaging (Shehzad et al., 2009), it has some limitations, which are, most notably, the high dependency upon the choice of a seed Region of Interest (ROI); the ROIs affected by the noise reduction approach (Murphy et al., 2009); and the disregard of relationships among multiple voxels.

In light of these issues, neuroimaging researchers have adopted a multivariate signal processing method known as Independent Component Analysis (ICA) to explore resting-state functional connectivity. ICA offers several advantages over seed-based correlation. First, ICA is a multivariate, data-driven approach. It thus requires no a priori hypothesis about brain activity models (Beckmann et al., 2005). Second, it detects interacting networks of regions, rather than just a single region-dominant (seed-ROI) network, by taking account of multiple simultaneous voxel-voxel relationships. Finally, this method is capable of extracting noise automatically such as scanner noise, physiological and motion artifacts(Thomas et al., 2001).

However even though ICA provides robust methodology for investigating functional connectivity it cannot describe its effectiveness (Liao et al., 2010; Deshpande et al., 2009). This effectiveness, or neurodynamics represents temporal causal effect dependencies between RSNs. Neurodynamics of a brain can be visualized using the Wiener-Granger causality test (Bressler and Seth, 2011) based on Granger's economical causality theory (Granger, 1969). Indeed, this statistical test allows us to determine whether one time series is useful in forecasting another. In other words, we state that a signal $X$ Granger-causes a signal $Y$ if the past of $X$ does convey information about the future of $Y$ above and beyond all information contained in the past of $Y$ (Seth, 2010). Signals $X$ and $Y$ represent time series of coactivated neuronal populations which are, in our case, the temporal trends of the RSNs.

The challenge in autism is to find relevant disparities with neurotypical people at rest, and thus be able to find biomarkers in the brain for ASD. However we hypothesize that the differences would be on the very subtle functional level and so maybe not in the composition of the network (connectivity) but in their interaction (causal effect). This is, to our knowledge, the first investigation trying to answer the following research question:

*"Are functional connectivity and neural dynamics different between high-functioning adolescents with ASD and typically developing controls at rest?"*

## 2. Materials and methods

### *2.1. Participants*

15 adolescents with ASD and 18 control adolescents participated in this study. Due to signal distortions caused by their braces, 2 adolescents with ASD and 5 control individuals were excluded from data analysis. All adolescents were between 12 and 18 years old. Adolescents with ASD were recruited from De Berkenschutse, a special secondary education school in Heeze (the Netherlands). All adolescents in the control group were recruited from regular secondary schools in other regions of our country.

Inclusion criteria for the adolescents with HFA were: established diagnostic criteria according to the DSM-IV as well as the autism algorithm cut-offs on the ADOS. Inclusion criteria for the control group were: no history of psychological or psychiatric illness. Exclusion criteria were: a (additional) diagnosis for a psychological or psychiatric illness as formulated in the DSM-IV, such as attention deficit and disruptive behavior disorders, separation anxiety disorders, selective mutism, reactive attachment disorder of infancy or early childhood, anxiety disorders and mood disorders; appearance of additional variables that can influence cognitive functioning such as pathology of the central nervous system, and a significant visual or hearing impairment.

Table 1 shows the means and standard deviations (SD) of the ages in months and the Wechsel following IQ scores: the Verbal Comprehension Index (VCI), Perceptual Organization Index (POI), Freedom from Distractibility Index (FDI) and Full Scale Intelligence Quotient (FSIQ). Using Multivariate Analysis of Variance (MANOVA) statistical method, we assessed the differences of the conditions (intelligence scores) of the both groups.

The study protocol was approved by the Medical Ethical Commission of the Maastricht University Medical Center.

### *2.2. Image acquisitions*

MRI imaging was performed on a 3.0-tesla unit equipped with an 8-channel receiver-only head coil (Philips Achieva, Philips Medical System, Best, The Netherlands). For anatomical reference, a transverse oriented T1-weights 3D Magnetization Prepared Rapid Acquisition with Gradient Echo (MPRAGE) was acquired with the folowing parameters: repetition time (TR) 8.2 ms, echo time (TE) 3.7 ms, flip angle 8 °, field of view (FOV) 240x240 $mm^2$, 150 slices, resolution 1x1x1 $mm^3$.

Then, resting-state fMRI data were acquired using the whole brain single-shot multi-slice BOLD echo-planar imaging (EPI) sequence, with TR 2 s, TE 35 ms, flip angle 90°, transverse orientation, matrix 128x128, FOV 256x256

**Tab. 1.** Demographic and descriptive data of ASD and typical control adolescents.

| Measure | Controls Mean (SD) | ASD Mean (SD) | Difference F(1,24) | p value* |
|---|---|---|---|---|
| Gender | 12 males, 1 female | 12 males, 1 female | | |
| Age (in months) | 173.9 (15.9) | 184.0 (14.2) | 2.89 | 0.102 |
| VCI | 117 (10.4) | 117.1 (9.0) | 0.0 | 0.968 |
| POI | 109.1 (7.8) | 114.0 (5.8) | 4.85 | 0.038 |
| FDI | 101.9 (14.6) | 99.5 (14.5) | 0.19 | 0.670 |
| FSIQ | 113.2 (7.8) | 116.7 (5.0) | 1.92 | 0.179 |

A $p - value < 0.05$ means that a score or a characteristic (rows of the table) differs significantly between the two groups.
** corrected for multiple comparison.*

mm$^2$, voxel size 2x2x4 mm$^3$, 31 contiguous slices per volume, and 210 volumes per acquisition; resulting in total resting-state acquisition of 7 minutes (210 volumes x 2 seconds). These resting-state scans have been performed twice with a 1-back test for working memory assessment in-between.

For the both resting-state scans, participants were instructed to lie with their eyes closed, to think of nothing and not to fall asleep.

### *2.3. Data preprocessing*

Data analysis was carried out using FMRIB Software Library (FSL)[1]. The following preprocessing was applied: discard of the first 3 volumes (= 6 s) allowing the MR signal to reach equilibrium; rigid-body motion correction (Jenkinson et al., 2002) to corrects and adjust the head motion in the 6 degrees of freedom (DOF) (3 translations / 3 rotations); non-brain removal; slice timing correction using the Fourier-space time-series phase-shifting in order to put in phase the time-series of each voxels for each volume; registration to a standard space; spatial smoothing using a Gausian kernel of 4.0 mm full-width at half-maximum (FWHM); grand-mean intensity normalization of the entire 4D dataset by a single multiplicative factor; high-pass temporal filtering using Gaussian-weighted least-squares straight line fitting, wtih $\sigma = 50.0$ s (comparable with traditional linear high-pass filtering with a cut-off frequency of 0.01 Hz). To register fMRI to standard space, functional scans of each subject were first registered to the T1-weighted structural images which were registered to the Montreal Neurological Institute (MNI) space. The MNI152 template (2mm isotropic) was used.

After those preprocessing steps one autistic subject were excluded because of a bad registration; and the second scan of a neurotypical subject was rejected because of a too high head motion.

### *2.4. Group independent component analysis*

A single group-level ICA was performed across all subjects and all scans from both HFA and control groups (total of 49 fMRI acquisitions) using probabilistic ICA as implemented in FSL Multivariate Exploratory Linear Optimized Decomposition into Independent Components (MELODIC). First, the previously preprocessed 4D dataset was temporally transformed by concatenation into a single time series. This new 4D image was, then, separated into 34 independent components (ICs). The number of components (34) was manually chosen to provide optimal balance between the number of components required to capture the relevant RSNs while avoiding component splitting (separating each network into too many subnetworks) (Wang et al., 2011). To obtain the components, group probabilistic ICA processing steps were applied to the temporally concatenated 4D image: masking out non-brain voxels, voxel-wise de-meaning of the data, and normalization of the voxel-wise variance. Subsequently, the pre-processed data were projected into a 34-dimensional subspace using probabilistic Principal Component Analysis. Then these observations were decomposed into sets of vectors which describe signal variation across the temporal domain (time-courses), the session/subject domain and across the spacial domain (maps) by optimizing for non-Gaussian spatial source distributions using a fixed-point iteration technique (Hyvärinen, 1999). The resulting estimated component maps were divided by the standard deviation of the residual noise and thresholded at a posteriori probability threshold of $p > 0.5$ (i.e, an equal lost is placed on false positives and false negatives) by fitting a Gaussian/gamma mixture model to the histogram of intensity values (Beckmann et al., 2005).

### *2.5. Resting state networks selection*

11 group-IC maps (over our 34) were selected according to the following 3 steps.First, group-ICs with more than 33% of the estimated spectral power in high-frequencies ($> 0.1$ Hz) were excluded (Tyszka et al., 2013) to keep only networks within the low frequency range of 0.1-0.01 Hz (Lowe et al., 1998). Secondly, Smith and colleagues described the major co-varying networks in the resting brain and created a template of these RSNs widely used in resting-state fMRI studies (Smith et al., 2009). With this template and our remaining group-ICs, a function, using

[1] www.fmrib.ox.ac.uk/fsl

the'goodness-of-fit' approach (Greicius et al., 2004; Vanhaudenhuyse et al., 2010), was created and applied. This template-matching method calculated the average Z-score. Finally, the third step consisted in a visual inspection of each component's spatial profile, e.g., biological plausibility, comparability to patterns previously reported in ICA based studies, to ensure the consistency and the efficiency of the two previous steps.
Figure 1 shows the 11 RSNs (with their name) selected from the group-ICA components.

### 2.6. Spatial RSN analysis between groups

The first level of the voxel-wise group analysis was performed using dual-regression (Filippini et al., 2009). The aim of this process is to obtain, from the group-IC maps, subject-specific IC maps. Dual regression involves two General Linear Models (GLM) (Figure 2). First, the 34 group ICA component maps were used as spatial regressors against the preprocessed individual fMRI scans. This results in single-subject time courses for each component separately (Fig. 2, block 1). Then, the time courses were normalized to unit variance to test both the "shape" and "amplitude" of the RSN. In the second GLM, these individual normalized time courses were used as temporal regressors against the preprocessed individual fMRI scans. Subject-specific components were thus estimated (Fig. 2, block 2). We finally got 34 subject-specific IC maps for each subject's scan.
As there were two subject-specific spatial maps of an IC for each individuals (one per scan), before running final group-level analysis, we merged and averaged them. That was also performed only for the ICs representing the 11 previously selected networks (Fig. 1). This resulted in 11 subject-specific IC maps for each of the 25 subjects.
The second level of the group analysis consisted in getting the effects of within-group means and between-group differences. This was assessed using non-parametric permutation testing (Nichols and Holmes, 2002), with FSL's Randomize tool, controlling for multiple comparison incorporating threshold-free cluster enhancer (TFCE) (Smith and Nichols, 2009). Besides modeling regressors for each of the two groups, additional nuisance regressors describing age, IQ and gray matter volume were added to the model in the second experiment. Null distributions being unknown, non-parametric tests were used, and to reflect the between- and within-group effects, 5000 permutations (Nichols and Holmes, 2002) were performed testing the differences between groups (ASD>control; control>ASD) or group-mean consistencies (control group average> 0; ASD group average> 0). For each RSN, the resulting statistical maps were threshold at $p < 0.05$ family-wise error (FWE) corrected using the TFCE technique, which provides strong Type I error control. TFCE method provides improved sensitivity compared to other cluster- and voxel-based thresholding (Smith and Nichols, 2009).

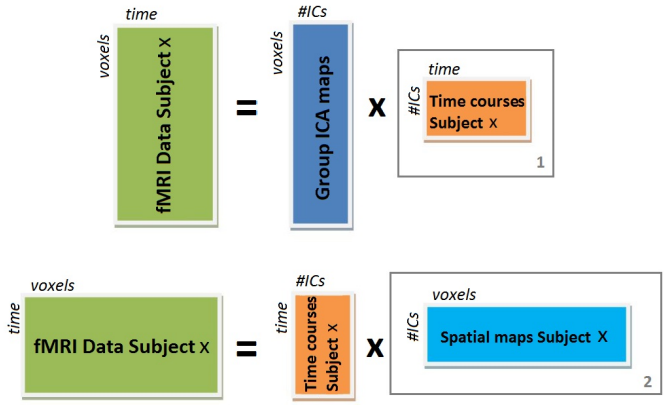


**Fig. 2.** Dual-regression steps. Block 1 shows individual time course resulting from the first step (spatial regression). Block 2 shows the single-subject IC maps resulting from the second step (temporal regression).

### 2.7. Temporal dynamics of RSN

The statistical Granger causality allows us to assess causality among two signals. One signal Y is said to Granger cause another signal X, if the past of Y and X can better predict the future of X rather than just with the past of X only (Zaremba and Aster, 2014). In this study we use this principle to evaluate pair-wise multivariate conditional Granger causalities of our independent components (resting-state networks). The assessment is made pair-wise, meaning that Granger causality will be performed on each couple of resting state networks. This assessment multivariate and conditional due to the fact that we have more than 2 networks (multivariate) and because the probability of having such causality between one network and another is depending of the past of those two signals and the additional information contributed by all the others networks. to measure a conditional G-causality, we use a Vector Autoregressive (VAR) model (Roebroeck et al., 2005; Zhou et al., 2009; Deshpande et al., 2011), which can be definied as

$$\mathbf{U}_t = \sum_{k=1}^{p} A_k \cdot \mathbf{U}_{t-k} + \boldsymbol{\varepsilon}_t \tag{1}$$

where $\boldsymbol{U}_t$ is a time serie vector, $A_k$ - regression coefficients, $\varepsilon$ - the residuals and $p$ - the model order representing the number of past lags taken into account. This model order is calculated from time series using the Akaike Information Criterion (AIC). Suppose we have

$$\mathbf{U}_t = \begin{pmatrix} \mathbf{X}_t \\ \mathbf{Y}_t \\ \mathbf{Z}_t \end{pmatrix}, \tag{2}$$

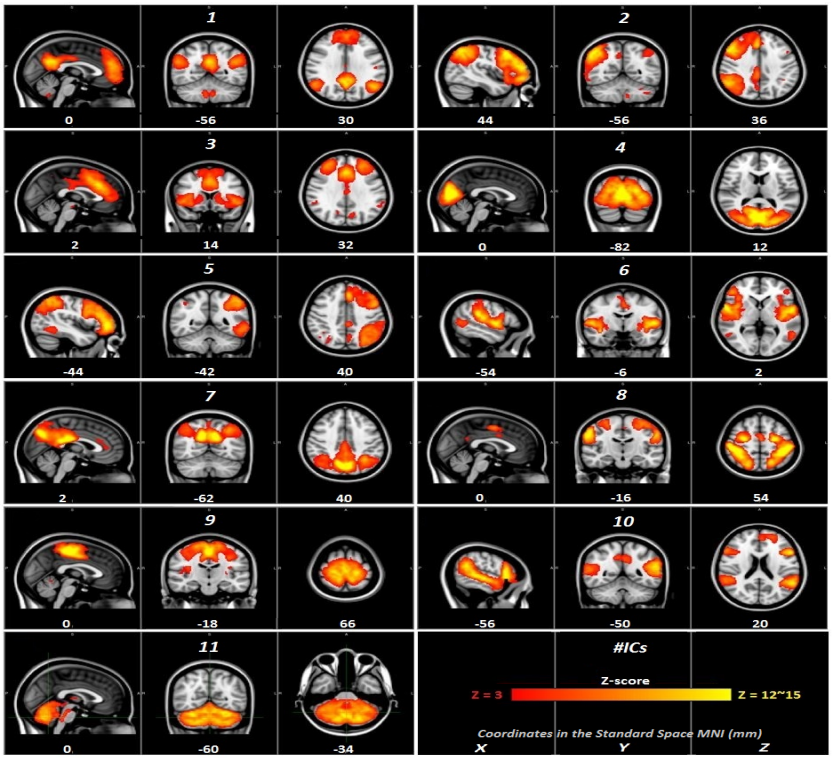


| #IC | Network |
|---|---|
| 1 | Default-mode |
| 2 | Fronto-parietal Right |
| 3 | Executive control |
| 4 | Visual system |
| 5 | Fronto-parietal Left |
| 6 | Auditory system |
| 7 | Precueus |
| 8 | Sensorimotor 1 |
| 9 | Sensorimotor 2 |
| 10 | Ventral stream |
| 11 | Cerebellum |

**Fig. 1.** Relevant components extracted from the 34 group ICA maps overlaid on the MNI standard brain (2x2x2mm). Names of the networks are in the right-side table. Colorbar is thresholded between 3 and 15 (z-score). MNI coordinates are in mm. The left hemisphere corresponds to the right side in the images (radiological convention).

where $\mathbf{X}_t$ and $\mathbf{Y}_t$ are two time series, and $\mathbf{Z}_t$ a third set of time series. we got from the VAR model (1)

$$\begin{pmatrix}\mathbf{X}_t\\ \mathbf{Y}_t\\ \mathbf{Z}_t\end{pmatrix} = \sum_{k=1}^{p}\begin{pmatrix}A_{xx,k} & A_{xy,k} & A_{xz,k}\\ A_{yx,k} & A_{yy,k} & A_{yz,k}\\ A_{zx,k} & A_{zy,k} & A_{zz,k}\end{pmatrix}\begin{pmatrix}\mathbf{X}_{t-k}\\ \mathbf{Y}_{t-k}\\ \mathbf{Z}_{t-k}\end{pmatrix} + \begin{pmatrix}\boldsymbol{\varepsilon}_{x,t}\\ \boldsymbol{\varepsilon}_{y,t}\\ \boldsymbol{\varepsilon}_{z,t}\end{pmatrix} \quad (3)$$

If we consider the $X$-component of the regression (4) we obtain the following expression:

$$\mathbf{X}_t = \sum_{k=1}^{p} A_{xx,k}\cdot\mathbf{X}_{t-k} + \sum_{k=1}^{p} A_{xy,k}\cdot\mathbf{Y}_{t-k} + \sum_{k=1}^{p} A_{xz,k}\cdot\mathbf{Z}_{t-k} + \boldsymbol{\varepsilon}_{x,t} \quad (4)$$

and if we suppose no conditional dependence between $\mathbf{X}$ and the past of $\mathbf{Y}$ ($A_{xy,1} = A_{xy,2} = \ldots = A_{xy,p} = 0$), we obtain the reduced regression

$$\mathbf{X}_t = \sum_{k=1}^{p} A'_{xx,k}\cdot X_{t-k} + \sum_{k=1}^{p} A'_{xz,k}\cdot\mathbf{Z}_{t-k} + \boldsymbol{\varepsilon}'_{x,t} \quad (5)$$

from that, we obtain the measure of the conditional Granger causality given by Geweke (Geweke, 1984):

$$F_{\mathbf{Y}\to\mathbf{X}|\mathbf{Z}} \equiv \ln\frac{|\Sigma'_{xx}|}{|\Sigma_{xx}|} \quad (6)$$

where $\Sigma'_{xx} = var(\boldsymbol{\varepsilon}'_{x,t})$ (4) is the variance of the prediction error (residuals) of $\mathbf{X}_t$ conditional on $\mathbf{Z}_t$ excluding the possible causal influence of $\mathbf{Y}_t$, and $\Sigma_{xx} = var(\boldsymbol{\varepsilon}_{x,t})$ (5) is the variance of the prediction error of $\mathbf{X}_t$ conditional on $\mathbf{Z}_t$, including also the possible causal influence of $\mathbf{Y}_t$. this equation (6) can be expressed as "the degree to which the past of $\mathbf{Y}$ helps predict $\mathbf{X}$ over and above the degree of which $\mathbf{X}$ is already predicted by its own past *and the past of* $\mathbf{Z}$" (Barnett and Seth, 2014).

After the dual-regression is performed, we take the individual IC time courses for each scan/subject (See Fig. 2, block 1). On these temporal trend of the RSNs we estimate, with the MVGC MATLAB toolbox (Barnett and Seth, 2014), the VAR model parameters $A_k$ and $\boldsymbol{\varepsilon}$. We obtain, thus, the conditional G-causality degree $F_{\mathbf{Y}\to\mathbf{X}|\mathbf{Z}}$ (6) for each scan of each patient and control, where $\mathbf{Y}$ and $\mathbf{X}$ are two RSN time series that we investigate directionally. in other words, we would like to answer the question: *does network Y G-cause X?* In our case, the G-causality is conditioned by all the other remaining RSN time series. Finally, with these 2-sample t-tests, we compare these G-causality magnitudes between the two groups (HFA vs controls) to discover different patterns of neuronal dynamics of the resting-state (effective connectivity). We perform the test for the two resting-state scan sessions to assess the reproducibility of such kind of G-causality tests. According to several studies, especially for task-based analysis, people with ASD get differences mainly in frontal and temporal cortices, and also in resting-state

brain connectivity within networks related to social interaction (Casanova et al., 2013; Wicker et al., 2008). Thus, we selected the 4 RSNs located mainly in fronto-temporal cortices and/or consisting of socio-cognitive brain parts. These networks are compounded with the default mode network, the executive system, the ventral stream and the auditory network. These networks are assessed and compared with the method described above.

## 3. Results

The results of adolescents' intelligence scores and their significant similarities between the two populations are displayed in Table 1. According to the p-values of this table, only the Perceptual Organization Index (POI) score showed a significant discrepancy between the adolescents with ASD and the TD controls ($p = 0.038 < 0.05$, Tab. 1)

### *3.1. Spatial RSN analysis between groups*

The presence of all the 11 networks was found in both HFA and neurotypical groups by testing the subject-specific maps of these networks (after the dual regression). Figure 3 shows the selected relevant networks, the group effects after a non-parametric permutation test (5000 permutations) thresholded at $p < 0.05$ TFCE corrected for FWE. These within-group inference maps showed a strong consistency with the whole group networks, when comparing Figures 1 and 3.
Even if, by observing their volume in average, some RSNs seem to be larger in the HFA population, no voxels in any component (the eleven relevant RSNs) survived at an FWE-corrected probability of 0.05 in the second-level group analysis for the ASD>control and control>ASD contrasts. In the second equivalent final statistical analysis, where age, IQ level and gray matter density were added as covariates, again, no voxels in any component survived at the same threshold. Table 2 shows thus that no p-values of the first voxels (at least one) activated (i.e. which show a difference between autism and control adolescents) is equal or less than 0.05.
The results confirm that, statistically, the strength and the breadth of each network (functional connectivity) was similar between both groups, i.e., no distinction could be made between high-functioning adolescent with ASD and neurotypical adolescents in their functional connectivity at rest.

### *3.2. Temporal dynamics of RSN*

Pairwise conditional Granger-causality magnitudes, in average, within each group for the 1st and 2nd resting-state scan sessions, are significant (p<0.05 FDR corrected) . This was found for the 4 selected prefrontal RSNs and for both groups. Also, the positivity of the normality test (Kolmogorov-Smirnov) for the distribution of the causalities among each group, allowed us to use the 2-sample t-test to compare HFA adolescents' G-causalities with those of the TD group.

In the 1st scan, none of the pairwise causalities differs significantly between ASD and TD adolescents. Same results are highlighted when comparing causalities within the TD group (1st scan vs 2nd scan).

However, dynamical RSN patterns do differ within the ASD cohort (1st scan vs 2nd scan) and significantly diverge from TD adolescent only for the 2nd resting-state scan. the latter describes, indeed, a weaker dynamical (cause/effect) relation between the ventral stream and executive control networks, especially in the direction from ventral stream to executive netw Figure 4 shows this causal connection between the 2 networks (ventral and executive) which differ between the groups during the 2nd resting-state scan. Figure 4 shows this comparison, i.e., the differences of the RSN temporal dynamics for the 2nd resting-state scan session including the 4 selected RSNs.

## 4. Discussion

In the present study of high-functioning adolescents with autism, whole-brain functional connectivity at rest was examined. No evidence concerning any significantly different connectivity is shown between the two populations at rest. These findings challenge the theory that the autistic brain is globally underconnected (Belmonte et al., 2004). this also contradict other literatures (Casanova et al., 2013). This is explained by the difference in scan protocols, in the method used (ICA vs seed-based) and mainly because of the population (type of the ASD, number and ages). Indeed this is, to our knowlege, the only resting-state fMRI analysis adolescent, from 12 to 18 years old, with HFA. Only one paper investigating resting-state in HFA adult population using ICA presented similar results of no differences in functional brain connectivity.

However, concerning neurdynamics, patterns of causal connectivity differ between HFA and controls and also between the 1st and 2nd scans for high-functioning ASD patients. Results show clearly that the patterns in neurodynamics, i.e. causal effects of one RSN on another, differ between the groups. Also, this neurodynamics changes in adolescents with HFA between the 1st and the 2nd resting-state scans, which does not happen for TD adolescents. In our study, there was is a memory task-based scan in between the two resting-state scan sessions. Therefore, we hypothesize that neurodynamical abnormal patterns were triggered by the previous task. For us, this task was the 1-back memory test (Barendse et al., 2013), triggering working memory, attentional and emotional (in face recognition) processes. The two RSNs showing differences in effective directed connectivity are the ventral stream and the executive control network. Ventral stream contains mainly the superior temporal sulci left and right, the

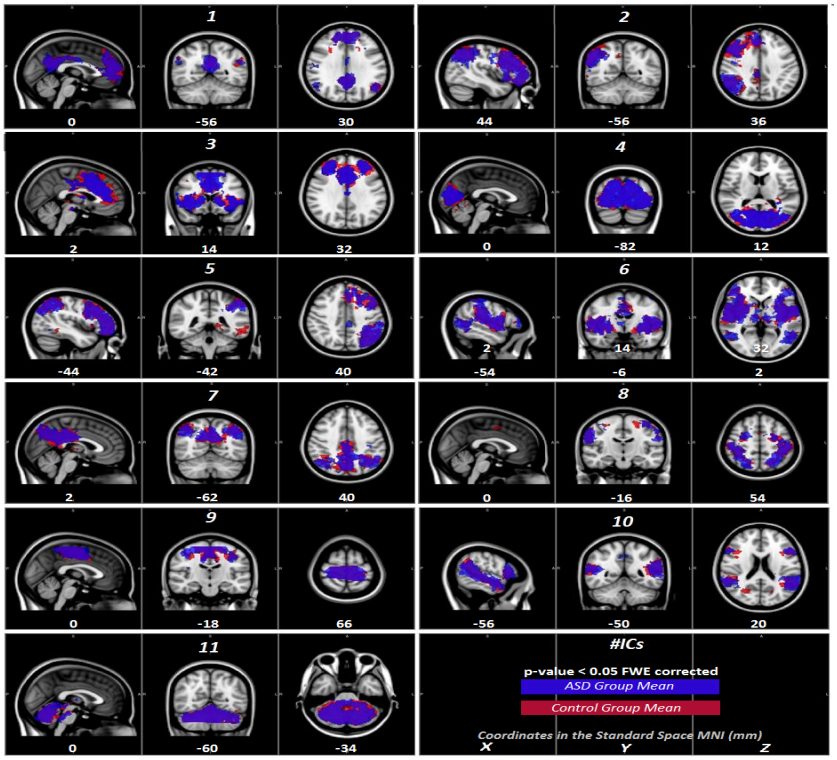


| #IC | Network |
|---|---|
| **1** | Default-mode 1 |
| **2** | Fronto-parietal Right |
| **3** | Executve control |
| **4** | Visual system |
| **5** | Fronto-parietal Left |
| **6** | Auditoy system |
| **7** | Precuneus |
| **8** | Sensorimotor 1 |
| **9** | Sensorimotor 2 |
| **10** | Ventral stream |
| **11** | Cerebellum |

**Fig. 3.** Group mean effect for each network. Blue = ASD mean; Red = Control mean; threeshold at $p < 0.05$ FWE corrected

**Tab. 2.** FWE-corrected P-values of the first voxels ($\geq 1$) showing a between-group difference.

| **Network** | p-value $Con > ASD$ | p-value $ASD > Con$ | p-value $Con > ASD$ adj* | p-value $ASD > Con$ adj* |
|---|---|---|---|---|
| **Default-mode 1** | 0.9275 | 0.535 | 0.84875 | 0.58 |
| **Fronto-parietal R** | 0.9355 | 0.125 | 0.585 | 0.23 |
| **Executve control** | 0.385 | 0.36 | 0.6525 | 0.6625 |
| **Visual system** | 0.325 | 0.83 | 0.38 | 0.74 |
| **Fronto-parietal L** | 0.285 | 0.6025 | 0.1 | 0.375 |
| **Auditoy system** | 0.96725 | 0.59 | 0.79125 | 0.6125 |
| **Precuneus** | 0.39 | 0.9385 | 0.13 | 0.815 |
| **Sensorimotor 1** | 0.205 | 0.7075 | 0.6 | 0.43 |
| **Sensorimotor 2** | 0.5475 | 0.21 | 0.78 | 0.175 |
| **Ventral stream** | 0.115 | 0.8994 | 0.255 | 0.9585 |
| **Cerebellum** | 0.77125 | 0.7625 | 0.775 | 0.7625 |

adj* = statistical maps adjusted for ages, IQ levels and gray matter volumes of subjects

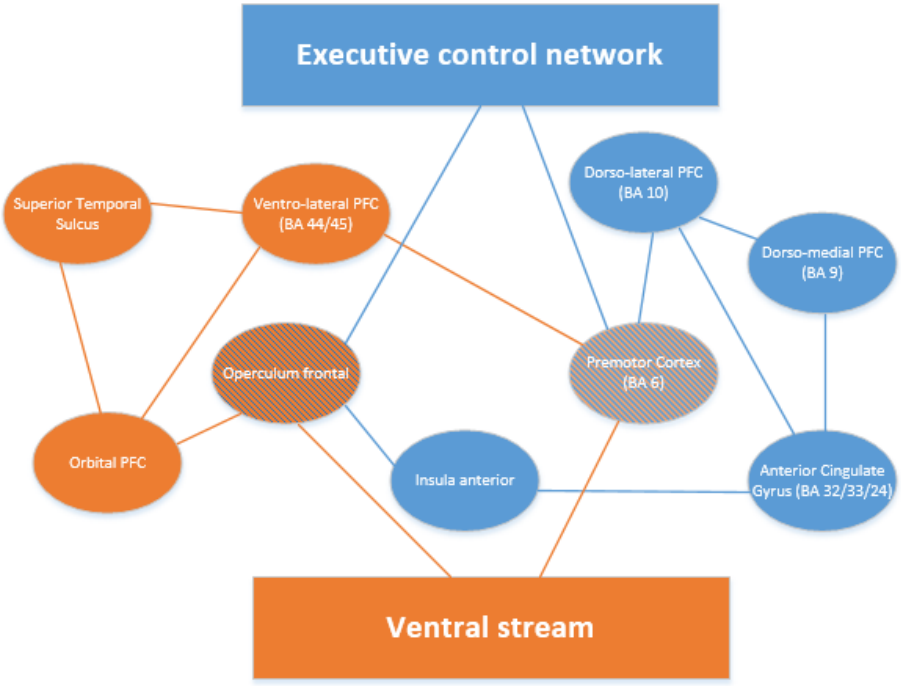


**Fig. 4.** Visualisation of the 2 RSNs - Executive in blue and ventral stream in orange- where causal dynamics are weaker in the direction from ventral to executive.

ventro-lateral and orbitall cortices, and parts of the pre-motor cortex. This pathway is known to code for visual recognition/identification and emotional process (part of limbic system). The executive control network involves the anterior cingulate gyrus, as well as the dorso-medial and dorso-lateral prefontal cortices, and also a piece of premotor cortex. Those regions of interest (ROI) involve cognitive processes such as working memory, reasoning, task flexibility, problem solving as well as planning and executing(Chan et al., 2008). This suggests that causal effect inferences between the two networks coding for those cognitive processes are significantly less involved for the adolescents with HFA (Barendse et al., 2013; Wicker et al., 2008). This can be understood as HFA adolescents keep a restrictive behavior even after the task.

Application of G-causality to fMRI BOLD has been highly controversial. One of the main issue often discussed is the problem of the Hemodynamic Response Function (HRF) changes. Inter-regional HRF variation has been argued to be particularly devastating for G-causality analysis (David et al., 2008). But the Grange causality method implemented in MVGC software is proved to be robust to changes in HRF properties (Seth et al., 2013). Also, the spectral density of our ICs being in the range of 0.01 and 0.1 Hz, the HFR phenomenon (between 4 and 10 seconds) does not appear in our RSNs signals before the G-causality analysis.

The second issue often mentioned in literature are the long sample intervals (TR) of classic fMRI protocols (usually ranging from 1 s to 3 s). Indeed, our TR=2 s, is substantially longer than typical inter-neuron delays. Though, as we examine changes (of differences) in G-causality rather than attempting to find a ground truth G-causality pattern, those issues alleviate (Barnett and Seth, 2014). Other issues for the G-causality analysis are related to task-based fMRI analysis, especially concerning the stationarity and the stochasticity of task-related signals (Bressler and Seth, 2011). But they do not affect resting-state analysis, as signals are supposed to be stationary and stochastic at rest.

Finally, for future applications, we think that this method is interesting and trustworthy only when ICA group analysis does not display any differences. Indeed, as we took the time courses of the ICs, it makes sense to analyze their G-causalities, only if they do not firstly differ spatially. Or in the contrary case (spatial differences in ICs between the two cohorts), we advise to use the raw time series of the voxels within an ROI (same for both groups) as Granger input signals.

## 5. Conclusion

We find no significant differences in brain connectivity between high-functioning adolescents with ASD and the control group at the whole-brain level. Adding age, IQ, and gray matter volumes as covariates did not change our

results.The extracted RSNs do not have the same pattern of dynamics, i.e., the influence of one RSN on another is different between the two cohorts. In particular, the causal connectivity between the executive control network and the ventral stream (mainly in the direction of ventral → executive) is significantly weaker in the HFA population in the 2nd resting-state sca These two networks link cortices coding for face/object recognition and emotional processing with cortices of executive cognitive functions (attention, control, working-memory, behavior). We conclude that changes in neurodynamics at rest in HFA is subtly triggered b rforming a task prior to resting-state analysis. And these changes appear in the networks related to the previous task.

Therefore, this study leads to the conclusion that brain connectivity in HFA population cannot be seen as globally abnormal, however networks of this connectivity have abnormal effectiveness (dynamics) at rest after a cognitive task for adolescents with HFA.

## References


Anderson JS, Nielsen JA, Froehlich AL, DuBray MB, Druzgal TJ, Cariello AN, Cooperrider JR, Zielinski BA, Ravichandran C, Fletcher PT, Alexander AL, Bigler AD, Lange N, Lainhart JE. Functional connectivity magnetic resonance imaging classification of autism. Brain 2011;134(12):3742–54. URL: http://brain.oxfordjournals.org/content/134/12/3742.

Barendse EM, Hendirks MP, Jansen JF, Backes WH, Hofman PA, Thoonen G, Kessels RP, Aldenkamp AP. Working memory deficits in high-functioning adolescents with autism spectrum disorders: neuropsychological and neuroimaging correlates. J Neurodev Disord 2013;5(14):1–11. URL: http://www.jneurodevdisorders.com/content/5/1/14.

Barnett L, Seth AK. The mvgc multivariate granger causality toolbox: A new approach to granger-causal inference. J Neurosci Methods 2014;223:50–68.

Beckmann CF, DeLuca M, Devlin JT, Smith SM. Investigation into resting-state connectivity using independent component analysis. Phil Trans R Soc B 2005;360(1457):1001–13. URL: http://www.ncbi.nlm.nih.gov/pubmed/16087444.

Belmonte MK, Allen G, Beckel-Michener A, Boulange LM, Carper RA, Webb SJ. Autism and abnormal development of brain connectivity. J Neurosci 2004;24(42):9228–31. URL: http://www.jneurosci.org/content/24/42/9228.full.

Bressler SL, Seth AK. Wiener-granger causality: A well established methodology. NeuroImage 2011;58(2):323–9.

Casanova MF, El-Baz AS, Suri JS. Imaging the brain in Austism. Springer, 2013.

Chan RC, Shum D, Toulopoulou T, Chen EY. Assessment of executive functions: Review of instruments and identification of critical issues. Archives of Clinical Neuropsycho 2008;23(2):201–16.

Cherkassky VL, Kana RK, Keller TA, Just MA. Functional connectivity in a baseline resting-state network in autism. NeuroReport 2006;17(16):1687–90. URL: http://www.ccbi.cmu.edu/reprints/Cherkassky_NeuroReport2006-fixation_preprint.pdf.

David O, Guillemain I, Saillet S, Reyt S, Deransart C, Segebarth C, Depaulis A. Identifying neural drivers with functional mri: an electrophysiological validation. PLoS Biol 2008;6(12):2683–97.

Deshpande G, LaConte S, Jamas GA, Peltier S, Hu X. Multivariate granger causality analyisis of fmri data. Hum Brain Mapp 2009;30(4):1361–73.

Deshpande G, Santhanam P, Hu X. Instantaneous and causal connectivity in resting state brain networks derived from functional mri data. NeuroImage 2011;54(2):1043–52.

Filippini N, j. MacIntosh B, Hough MG, Goodwin GM, Frisoni GB, Smith SM, Matthews PM, Beckmann CF, Mackay CE. Distinct patterns of brain activity in young carriers of APOE-$\varepsilon$4 allele. Proc Natl Acad Sci USA 2009;106(17):7209–14. URL: http://www.pnas.org/content/early/2009/04/08/0811879106.

Geweke JF. Measure of conditional linear dependence and feedback between time series. J Am Stat Assoc 1984;79(388):907–15.

Granger CWJ. Investigating causal relations by econometric models and cross-spectral methods. Econometrica 1969;37(3):424–38.

Greicius MD, Srivastava G, Reiss AL, Menon V. Default-mode network activity distinguishes Alzheinmer's disease from healthy aging: Evidence from functional mri. Proc Natl Acad Sci USA 2004;101(13):4637–42. URL: http://www.pnas.org/content/101/13/4637.

Hyvärinen A. Fast and robust fixed-point algorithms for independent component analysis. IEEE Trans Neural Netw 1999;10(3):626–34. URL: http://www.cs.helsinki.fi/u/ahyvarin/papers/TNN99new.pdf.

Jenkinson M, Bannister P, Brady M, Smith S. Improved optimization for the robust and accurate linear registration and motion correction of brain images. NeuroImage 2002;17(2):825–41. URL: http://www.ncbi.nlm.nih.gov/pubmed/12377157.

Liao W, Mantini D, Zhang Z, Pan Z, Ding J, Gong Q, Yang Y, Chen H. Evaluating the effective connectivity of resting state networks using conditional granger causality. Biol Cybern 2010;102(1):57–69.

Lowe MJ, Mock B, Sorenson J. Functional connectivity in single and multislice echoplanar imaging using resting-state fluctuations. NeuroImage 1998;7(2):119–32. URL: http://www.sciencedirect.com/science/article/pii/S1053811997903153.

Möller RA, Shilh P, Keehn B, Deyoe JR, Leyden KM, Shukla DK. Underconnected, but how? a survey of functional connectivity mri studies in autism spectrum disorders. Cerebral Cortex 2011;21(10):2233–43. URL: http://www.ncbi.nlm.nih.gov/pmc/articles/PMC3169656/.

Monk CS, Peltier SJ, Wiggins JL, Weng SJ, Carrasco E, Risi S, Lord C. Abnormalities of intrinsic functional connectivity in autism spectrum disorders. Neuroimage 2009;47(2):764–72. URL: http://www.ncbi.nlm.nih.gov/pubmed/19409498.

Murphy K, Bim RM, Handwerker DA, Jones TB, Bandettini PA. The impact of global signal regression on resting state correlations: Are anti-correlated networks introduced. NeuroImage 2009;44(3):893–905. URL: http://www.ncbi.nlm.nih.gov/pmc/articles/PMC2750906/.

Nichols TE, Holmes AP. Nonparametric permutation tests for functional neuroimaging: a primer with example. Hum Brain Mapp 2002;15(1):1–25. URL: http://www.ncbi.nlm.nih.gov/pubmed/11747097.

Roebroeck A, Formisano E, Goebel R. Mapping directed influence over the brain using granger causality and fmri. NeuroImage 2005;25(1):230–42.

Seth AK. A matlab toolbox for granger causal connectivity analysis. J Neurosci Meth 2010;186(2):262–73.

Seth AK, Chorley P, Barnett L. Granger causality analysis of fmri bold signals is invariant to hemodynamic convolution but not downsampling. NeuroImage 2013;65:540–55.

Shehzad A, Kelly AMC, Reiss PT, Gee DG, Gotimer K, Uddin LQ, Lee SH, Margulies DS, Roy AK, Bisxal BB, Petkova E, Castellanos FX, Milham MP. The resting brain: Unconstrained yet reliable. Cerebral Cortex 2009;19(10):2209–29. URL: http://cercor.oxfordjournals.org/content/19/10/2209.long.

Smith SM, Fox PT, Miller KL, Glahn DC, Fox PM, Mackay CE, Filippini N, Watkins KE, Toro R, Laird AR, Beckmann CF. Correspondence of the brain's functional architecture during activation and rest. Proc Natl Acad Sci USA 2009;106(31):13040–5. URL: http://www.pnas.org/content/early/2009/07/17/0905267106.

Smith SM, Nichols TE. Threshold-free cluster enhancement: adressing problems of smoothing, threshold dependence and localisation in cluster inference. NeuroImage 2009;44(1):83–98. URL: http://www.ncbi.nlm.nih.gov/pubmed/18501637.

Soulière I, Dazson M, Gernsbacher MA, Mottron L. The level and

nature of autistic intelligence ii: What about asperger syndrome? PLoS one 2011;(9).

Thomas CG, Harshman RA, Menon RS. Noise reduction in bold-based fmri using component analysis. NeuroImage 2001;17(3):1521–37. URL: http://www.sciencedirect.com/science/article/pii/S1053811902912000.

Tyszka JM, Kennedy DP, Paul LK, Adolphs R. Largely typical patterns of resting-state functional connectivity in high-functioning adults with autism. Cerebral Cortex 2013;:1–12URL: http://cercor.oxfordjournals.org/content/early/2013/02/20/cercor.bht040.full.pdf+html.

Vanhaudenhuyse A, Noirhomme Q, Tshibanda LJF, Bruno MA, Boveroux P, Shnakers C, Soddu A, Perlbarg V, Ledoux D, Brichant JF, Moonen G, Maquet P, Greicius MD, Laureys S, Boly M. Default network connectivity reflects the level of consciousness in non-communicative brain damaged patients. Brain 2010;133(1):161–71. URL: http://www.ncbi.nlm.nih.gov/pubmed/20034928.

Wang X, Foryt P, Ochs R, Chung JH, Wu Y, Parrish T, Ragin AB. Abnormalities in resting-state functional connectivity in early Human Immunodeficiency Virus infection. Brain Connectivity 2011;1(3):207–2017. URL: http://www.ncbi.nlm.nih.gov/pubmed/22433049.

Wicker B, Fonlupt P, Hubert B, Tardif C, Gepner B, Deruelle C. Abnormal cerebral effective connectivity during explicit emotional processing in adults with autism spectrum disorder. Soc Cogn Affect Neurosci 2008;3(2):135–43.

Zaremba A, Aster T. Measures of causality in complex datasets with application to financial data. Entropy 2014;16(4):2309–49.

Zhou Z, Wang X, Klahr NJ, Liu W, Arias D, Liu H, von Deneen Ying Wen KM, Lu Z, Xu D, Liu Y. A conditional granger causality model approach for group analysis in functional magnetic resonance imaging. Magn Reson Imaging 2009;29(3):418–33.

Zuo XN, Kelly C, Adelstein JS, Klein DF, Castellanos FX, Milham MP. Reliable intrinsic connectivity network: Test-retest evaluation using ica and dual regression approach. NeuroImage 2011;49(3):2163–77. URL: http://www.ncbi.nlm.nih.gov/pmc/articles/PMC2877508/.